Journal of Nuclear Medicine, published on June 28, 2019 as doi:10.2967/jnumed.119.226712

PET imaging of tumor PD-L1 expression with a highly specific non-blocking nanobody

Gaochao Lv[1], Ling Qiu[1*], Yan Sun[2], Ke Li[1], Qingzhu Liu[1], Qi Zhao[3], Songbing Qin[3*], Jianguo Lin[1*]

[1]*Key Laboratory of Nuclear Medicine, Ministry of Health, Jiangsu Key Laboratory of Molecular Nuclear Medicine, Jiangsu Institute of Nuclear Medicine, Wuxi, China;*

[2]*Smart Nuclide Biotech, Suzhou, China;*

[3]*Department of Radiation Oncology, First Affiliated Hospital of Soochow University, Suzhou, China.*

First author: Dr. Gaochao Lv, E-mail: lvgaochao@jsinm.org

***Corresponding author**: Dr. Jianguo Lin, E-mail: linjianguo@jsinm.org; Dr. Ling Qiu, E-mail: qiuling@jsinm.org

Dr. Gaochao Lv, Dr. Jianguo Lin and Dr. Ling Qiu share address: Key Laboratory of Nuclear Medicine, Ministry of Health, Jiangsu Key Laboratory of Molecular Nuclear Medicine, Jiangsu Institute of Nuclear Medicine, Wuxi 214063, China. Phone: +86(510)-85514482.

OR

Dr. Songbing Qin, E-mail: qin92244@163.com

Department of Radiation Oncology, First Affiliated Hospital of Soochow University, Suzhou, China.

Running title: ^{68}Ga-labeled PD-L1 targeted nanobody

Word count: 4998

ABSTRACT

Rationale: Although immunotherapy through programmed death 1 / programmed death ligand 1 (PD-1/PD-L1) checkpoint blockade has shown impressive clinical outcomes, not all patients respond to it. Recent studies have demonstrated that the expression level of PD-L1 in tumors is one of the factors that correlate with the PD-1/PD-L1 checkpoint blockade therapy. Herein, a novel ^{68}Ga-labeled nanobody tracer, ^{68}Ga-NOTA-Nb109, was designed and developed for specific and noninvasive imaging of PD-L1 expression in the melanoma-bearing mice model.

Methods: The nanobody Nb109 was labeled with the radionuclide ^{68}Ga through a NOTA chelator. In vitro binding assay was performed to assess the affinity and binding epitope of Nb109 to PD-L1. The clinical application value of ^{68}Ga-NOTA-Nb109 was evaluated by the stability assay, biodistribution and pharmacokinetics studies as well as positron emission tomography (PET) imaging, autoradiography and immunohistochemical staining studies on the tumor-bearing models with different PD-L1 expression.

Results: The tracer ^{68}Ga-NOTA-Nb109 was obtained with the radiochemical yield > 95% and the radiochemical purity > 98% in 10 min. It showed a high specific affinity for PD-L1 with the equilibrium dissociation constant (K_D) of 2.9×10^{-9} M. A competitive binding assay indicated a different binding epitope for Nb109 compared with PD-1 and PD-L1 antibody. All the biodistribution, PET imaging, autoradiography and immunohistochemical staining studies revealed that the tracer ^{68}Ga-NOTA-Nb109

specifically accumulated in A375-hPD-L1 tumor with a maximum uptake of 5.0 ± 0.35 %ID/g at 1 h.

Conclusions: The tracer ^{68}Ga-NOTA-Nb109 holds great potential for noninvasive PET imaging of the PD-L1 status in tumors and timely evaluating the therapeutic effect of immune checkpoint targeting treatment.

Key Words: Immune checkpoints, PD-L1, Positron emission tomography, Nanobody tracer

INTRODUCTION

Immune checkpoints are inhibitory pathways of the immune system that maintain self-tolerance and prevent autoimmunity (*1*). One of the checkpoint receptors, programmed cell death protein-1 (PD-1), has been widely studied in the context of clinical cancer immunotherapy, which serves as a negative regulator of T-cells (*2*). Upon binding to either of its two ligands, PD-L1 or PD-L2, PD-1 will initiate an inhibitory signaling cascade through its intracellular signaling domains, including an immunoreceptor tyrosine-based inhibitory motif and immunoreceptor tyrosine-based switch motif (*3*). By up-regulating the expression level of PD-L1, tumor cells are capable of escaping immune recognition and attack (*4*). Recently, several immunotheraputic antibodies that block the PD-1/PD-L1 pathway have shown encouraging results in clinical applications, such as nivolumab, pembrolizumab, and atezolizumab et.al (*5*). The remarkable results prompted Food and Drug Administration to accelerate approval of pembrolizumab and nivolumab for the treatment of advanced melanoma in late 2014, and nivolumab was also approved for the treatment of non-small cell lung carcinoma in early 2015 (*6*).

Unfortunately, although immunotherapy targeted PD-1/PD-L1 pathway shows impressive clinical outcomes, not all patients respond to this type of treatment (*7*). Several studies have demonstrated that the expression level of PD-L1 in tumors might be one of the factors that correlate with the PD-1/PD-L1 checkpoint blockade therapy (*8-10*). Thus, it is essential to analyze the PD-L1 expression in patients prior to treatment, which

may avoid the ineffective cure and improve the success rate of immunotherapy. The traditional method immunohistochemistry is limited on the analysis of PD-L1 expression in tumors because of the highly dynamic and heterogeneous expression of checkpoint molecules (*11*). Thus, there is an urgent need for real-time, dynamic and exact detection of PD-L1 with high sensitivity and resolution (*12*). Recently, positron emission tomography (PET) imaging with radiolabeled anti-PD-L1 antibodies showed important advantages on the detection of PD-L1 expression over immunohistochemistry (*13*). Besides the operator-independent procedure, both primary tumor and metastases can be evaluated by a single noninvasive whole-body imaging procedure, thereby avoiding sampling errors in the case of PD-L1 expression heterogeneity (*14*). Moreover, PET imaging also allows a more accurate quantitative assessment of the total amount of PD-L1 expression in an individual patient, which could provide important information for determining the treatment method or the dose of anti-PD-L1 therapy (*15-19*). However, the slow clearance rate of antibody agents often takes many days to clear sufficiently from soft tissues and enable imaging of the target (*20*). As an ideal PET imaging agent of PD-L1, it should offer high uptake in PD-L1-positive tumors and low background signal in a short time (*21*). Due to small size and favorable physicochemical properties, nanobodies have attracted considerable attentions which hold great potential in the design of PD-L1 targeting imaging agents (*22*).

Furthermore, except before treatment, the prognostic evaluation of the PD-L1 level is also crucial for monitoring the therapeutic effect (*23*). Notably, different binding site of

the tracer and anti-PD-L1 therapeutic antibodies is a popular trait for the prognostic evaluation, which could not be affected by the therapeutic antibodies in the course of treatment (*24*). Herein, we screened and identified a non-blocking nanobody with high specific affinity for PD-L1, namely Nb109. It was further conjugated with the chelator 1,4,7-triazacyclononane-1,4,7-triacetic acid (NOTA) and labeled by the radionuclide ^{68}Ga (Fig. 1). The tracer ^{68}Ga-NOTA-Nb109 showed promising clinical value in imaging of PD-L1 expression in xenograft tumors and held great potential applications for guiding immunotherapy.

MATERIALS AND METHOD

Materials

All reagents were obtained from Sigma-Aldrich unless otherwise stated. p-SCN-Bn-NOTA was purchased from Macrocyclics. The PD-L1 anti-body KN035 was kindly provided by Alphamab Co. Ltd (Suzhou, China). The mass spectra were measured by the high-resolution LTQ-Orbitrap XL mass spectrometer interfaced with a heated electrospray ionization source (Thermo Scientific, CA) and the data were treated by Thermo Biopharma Finder 3.0. ^{68}Ga was obtained from a ^{68}Ga/^{68}Ge generator (IGG-100, Eckert & Ziegler AG). High Performance Liquid Chromatography (HPLC) was performed on Waters 2998 with a SEC chromatogram (G3000SWXL, TOSOH).

Production and Purification of Nanobody

Anti-PD-L1 nanobody DNA fragments were re-cloned in a suitable mammalian expression vector pcDNA4 (Invitrogen, Cat V86220). Human embryonic kidney

suspension-adapted cells HEK293F were cultured according to standard protocols. Starter cultures (30-100 mL) were maintained in 250 mL conical cell culture flasks. To obtain transient co-transfection HEK293F cells, freestyle HEK293F cells were adapted to grow in suspension cultures, reaching high densities using serum-free media. And then the cells were transiently transfected using a branched version of polyethylenimine. Intracellular proteins were harvested by centrifuging cells at 3,000×g for 5 min. Nanobodies were further purified using immobilized affinity chromatography and ion-exchange liquid chromatography on SP resin (GE Healthcare), followed by buffer exchange to phosphate-buffered saline.

Synthesis of ^{69}Ga-NOTA-Nb109

The precursor NOTA-Nb109 was obtained by conjugation of p-SCN-Bn-NOTA with amino groups of Nb109 according to previous report (*11*). To a solution of $Ga(NO_3)_3$ (2.0 nmol) in 500 μL of 0.25 M sodium acetate, 0.05 M HCl was added to adjust the pH of reaction system to 4.0, followed by the addition of NOTA-Nb109 (100 μg). And then the mixture was incubated at room temperature for 10 min and purified with a PD-10 column.

Synthesis of the Probe ^{68}Ga-NOTA-Nb109

The radionuclide ^{68}Ga was eluted from a ^{68}Ga/^{68}Ge generator using 0.05 M HCl (5 mL) as the fractionated eluent. The nanobody Nb109 (100 μg) was mixed with the metallic cation $^{68}Ga^{3+}$ (1 mL) and sodium acetate (0.25 M, 225 μL). The reaction mixture was incubated at room temperature for 10 min and purified by PD-10 column with saline as the eluent.

The purity and stability of ^{68}Ga-NOTA-Nb109 was measured by the radio-HPLC/SEC chromatography using 0.01 M phosphate buffer (pH 7.4) as the mobile phase at the flow rate of 1 mL/min.

Binding Affinity Assay

The affinity of nanobody Nb109 for immobilized human PD-L1 protein was tested using surface plasmon resonance. All measurements were performed on a Biacore T200 device at 25 °C using Hepes-buffered saline (0.01 M HEPES pH 7.4, 0.15 M NaCl, 3 mM ethylenediaminetetraacetic acid, 0.005% Tween 20) as the running buffer. Briefly, 6 different dilutions of Nb109 (0.94, 1.85, 3.75, 7.5, 15, and 30 nM) were run at 50 μL/min on a CM5 sensor chip with high density of human PD-L1 protein and specific binding signals (response units, RU) were recorded. Nb109 dilutions were allowed to bind with the target protein for 300 sec and dissociation was monitored for 180 sec. The equilibrium dissociation constant K_D was calculated by fitting the obtained sensor grams to theoretical curves using Biacore Evaluation software.

The competition binding assay was performed by enzyme-linked immunosorbent assay (ELISA). PD-L1-muFc and PD-1-Fc were expressed by HEK293 cell lines (pcDNA4, Invitrogen，Cat V86220). PD-L1-muFc was coated on the plate as capture reagent by 0.5 μg per well. The plate was incubated at 4 °C overnight and the excess of uncoated fusion protein was removed by washing the plate three times with phosphate buffer containing 0.01% Tween 20. Subsequently, 10 μg PD-1-Fc was added followed by the addition of Nb109 with geometric dilution at the initial concentration of 100 μg/mL.

After incubation at room temperature for 1 h, 100 μL anti-his-HRP (Abcam) was added to the plate and then reacted for another 1 h. The ELISA was developed by adding 100 μL of 3,3',5,5'-tetramethylbenzine substrate and subsequent incubation for 25 min at room temperature. The plates were read at optical density 405 nm with a VersaMax ELISA Microplate Reader (Molecular Devices).

Cell Lines and Culture Conditions

Human melanoma cell line A375 and human PD-L1 gene transfected A375 cells (A375-hPD-L1) were kindly provided by Smart Nuclide Biotech (China) and cultured in Dulbecco's Modified Eagle Medium with 10% fatal bovine serum (Gibco), 100 U/mL penicillin and 0.1 mg/mL streptomycin. Human breast cancer cells MCF-7 were obtained from American Type Culture Collection (Manassas, USA). MCF-7 cells were cultured in Eagle's Minimum Essential Medium with 10% fatal bovine serum and 0.01 mg/ml human recombinant insulin (Sigma). All cells were grown in monolayer in falcon tissue culture dishes (Becton Dickinson, USA) and incubated at 37 °C in a humidified incubator with 5% CO_2.

Flow Cytometry for PD-L1 expression

The expression level of PD-L1 in A375-hPD-L1 and MCF-7 cell lines was analyzed using a PD-L1 monoclonal antibody (Clone 44716) conjugated to phycoerythrin. Flow cytometric analyses were performed on Beckman Coulter Cytomics FC 500 MPL (USA).

Cellular Uptake and Immunoreactivity

The cellular uptake was studied according to the previous report (*10*). The immunoreactive fraction was obtained by the Lindmo assay (*25*). For competitive binding

assay, the tumor cell (A375-hPD-L1) uptake of ^{68}Ga-NOTA-Nb109 was studied with or without pretreatment of a 1000-fold molar excess of unlabeled Nb109 or KN035. The PD-L1 antibody KN035 has been approved by investigational new drug for the treatment of advanced or metastatic solid tumors (NCT02827968, NCT03101488, and NCT03248843) (*4,26*).

Animal Studies

At 5-7 weeks of age, female BALB/c nude mice were inoculated subcutaneously with 1×10^6 A375-hPD-L1 or MCF-7 cells. To further demonstrate the PD-L1 targeting ability of ^{68}Ga-NOTA-Nb109 and eliminate individual differences, different cancer cells of A375-hPD-L1, the mixture of A375-hPD-L1/A375 (1/1, v/v) and A375 were simultaneously inoculated at the left hind leg, right hind-leg and right fore-leg of the same mouse subcutaneously, respectively. Experiments started when tumors reached a size of approximately 250~350 mm^3. All experiments for animal research were conducted in accordance with the principles laid out by the ethical committee of Jiangsu Institute of Nuclear Medicine.

MicroPET Imaging Studies

MicroPET imaging was performed on an Inveon microPET scanner (Siemens Medical Solutions, Germany). Xenograft nude mice were injected with 4.0-5.0 MBq ^{68}Ga-NOTA-Nb109 via tail vein. For the blocking group, the mice were pre-treated with the antibody KN035 (5 mg/kg) one day in advance. The mice were anesthetized with 1.5%–2% isoflurane in 0.5 L/min flow of oxygen. MicroPET static imaging (10 min) was

performed at 1, 2 and 4 h post injection. Dynamic images were collected for two hours. The obtained images were reconstructed using three-dimensional ordered subset expectation maximization (OSEM 3D/SP-MAP) without attenuation correction and then processed using the Siemens Inveon Research Workplace (IRW2.0.0.1050). Regions of interest were drawn over tumors and main organs, and average signal levels in the regions were measured.

Autoradiography and Immunohistochemical Staining for PD-L1 Expression

After injection of the tracer for 90 min, animals were processed for autoradiography and immunohistochemical staining as previous reports (*17,27*).

Biodistribution and Pharmacokinetics Studies

Mice with subcutaneous A375-hPD-L1 or MCF-7 xenografts were divided into two groups (n=5), respectively, and then received an intravenous injection of 3.7 MBq ^{68}Ga-NOTA-Nb109. At 1 and 2 h post injection, the mice were sacrificed and main organs were dissected, washed, weighed, and counted by a γ counter. The uptake of the radiotracer was expressed as percentage of injected dose per gram of tissue (%ID/g). For pharmacokinetics study, blood samples at different time points (0, 5, 15, 30, 60 and 120 min) were collected and counted using a γ counter. Statistical analysis was performed using Origin 7.5.

RESULTS

Synthesis and Characterization of ^{68}Ga-NOTA-Nb109

The molecular weight of the obtained nanobody Nb109 was about 14 KDa, which was further determined accurately to be 13612 (Supplemental Fig. 1). The conjugate NOTA-Nb109 was prepared by coupling p-SCN-Bn-NOTA with the lysine of anti-PD-L1 nanobody Nb109 (Fig. 2). Due to the existence of three lysine residues in the framework region of Nb109, a mixture of single- and double-NOTA chelator conjugated with per nanobody molecule was produced (Supplemental Fig. 2). The successful generation of the complex ^{69}Ga-NOTA-Nb109 was characterized by mass spectra (Supplemental Fig. 3).

Subsequently, the target tracer ^{68}Ga-NOTA-Nb109 was produced with radiochemical yield >95% and radiochemical purity >98% in sodium acetate buffer (pH = 4.0), and the molar activity was determined to be 25.17 ± 3.26 GBq/μmol (Supplemental Fig. 4A). In vitro stability of ^{68}Ga-NOTA-Nb109 in phosphate buffer and serum was demonstrated with the radiochemical purity of >98% over 4 h under 75 ℃ (Supplemental Fig. 4B,C). The immunoreactive fraction was determined to be 67.7 ± 4.8% for ^{68}Ga-NOTA-Nb109 (Supplemental Fig. 5).

In vitro Binding Assay of Nb109 to PD-L1

As shown in Fig. 3A, Nb109 exhibited a strong affinity for PD-L1 with the equilibrium dissociation constant (K_D) of 2.9 × 10^{-9} M, high binding rate constant (K_a = 1.6 × 10^5 1/Ms) and low dissociation rate constant (K_d = 4.9 × 10^{-4} 1/s). The typical S-type binding curves of Nb109 and ^{69}Ga-NOTA-Nb109 to PD-L1 by ELISA also

indicated the strong binding ability of Nb109 and ^{69}Ga-NOTA-Nb109 to PD-L1 (Supplemental Fig. 6).

A competitive binding assay showed that the presence of PD-1 has no influence on the binding of Nb109 with PD-L1, since the typical S-type binding curve between Nb109 and PD-L1 was observed (Fig. 3B). Meanwhile, the binding of Nb109 with PD-L1 also made no difference to the binding of PD-1 with PD-L1, as the binding curve between PD-1 and PD-L1 showed virtually no change. To confirm the results, we investigated whether KN035 competed with ^{68}Ga-NOTA-Nb109 to bind to A375-hPD-L1 cells. After pretreated with 1000-fold excess of KN035 for 30 min, the cellular uptake of ^{68}Ga-NOTA-Nb109 was comparable to that of untreated group in 4 h, but it significantly decreased from 7.17 ± 1.01% to 1.94 ± 0.53% by pretreatment with the same amount of unlabeled Nb109 (Fig. 3C). Furthermore, after pretreatment with 1000-fold KN035 for 0.5 to 4 h, the cellular uptake of ^{68}Ga-NOTA-Nb109 in A375-hPD-L1 was comparable with untreated group, as the ratio of pretreated /untreated group was always close to 1 (Fig. 3D).

The cell uptake of ^{68}Ga-NOTA-Nb109 at 2 h was 6.3 ± 0.31% and 1.3 ± 0.44% for A375-hPD-L1 (PD-L1-positive) and MCF-7 (PD-L1-negative) cells, respectively (Supplemental Fig. 7,8), which indicated the specificity of ^{68}Ga-NOTA-Nb109 to PD-L1 in tumor cells

MicroPET Imaging

As shown in Fig. 4A, A375-hPD-L1 tumor-bearing mice showed rapid and high

tumor uptake of 5.32 ± 0.47 %ID/g at 10 min post injection (Fig. 4B). The optimal images were observed at 1 h post injection with the highest tumor-to-muscle ratio of 11.03 ± 0.36 (Fig. 4C). However, MCF-7 tumors were not visible throughout the whole microPET imaging. As for the tumor A375-hPD-L1 bearing mice pre-treated with the antibody KN035 (5 mg/kg) for 24 h, the tumor uptake of ^{68}Ga-NOTA-Nb109 was comparable to that was injected with only ^{68}Ga-NOTA-Nb109 (Fig. 4A,B).

In addition, microPET static scanning was also performed on three types of tumor-bearing mice and shown in Fig. 5. As expected, A375-hPD-L1 tumor was clearly observed and showed the highest uptake of radioactivity (4.94±0.46 %ID/g) at 1 h (Fig. 5A,B). As for the tumor of mixture A375-hPD-L1/A375, the uptake was almost half less than that in A375-hPD-L1 tumor at all time points. And it was determined to be 3.06 ± 0.31 %ID/g at 1 h. As for the negative A375 tumor, the tumor was not visible throughout the scanning. The results correlated well with the PD-L1 expression determined by immunohistochemistry, as the PD-L1 positive area in A375-hPD-L1 and A375-hPD-L1/A375 tumors was determined to be 30 ± 6.36% and 15 ± 4.24% respectively (Fig. 5C). The results were further confirmed by ex vivo autoradiography of tumors post imaging (Fig. 5D).

Biodistribution and Pharmacokinetics Study

The biodistribution of ^{68}Ga-NOTA-Nb109 in A375-hPD-L1 and MCF-7 tumor-bearing mice was presented in Fig. 6. At 1 h post injection, the kidney showed relatively high uptake (33.66 ± 3.26 %ID/g), while the liver (1.11 ± 0.41 %ID/g) and

remaining organs (<1.5 %ID/g) showed low uptake. The tumor uptake in A375-hPD-L1-bearing mice was rapid and high (5.0 ± 0.35 %ID/g), but that in MCF-7-bearing mice was only 1.7 ± 0.36 %ID/g. At 2 h post injection, the tumor uptake in A375-hPD-L1 and MCF-7 bearing mice both decreased slightly to 4.05 ± 0.31 and 1.46 ± 0.34 %ID/g, respectively. The pharmacokinetics study showed that ^{68}Ga-NOTA-Nb109 could be cleared fast from the blood with a half-life of 49.79 min (Supplemental Fig. 9), which resulted in high tumor-to-muscle (T/M) (9.33 ± 0.82) and tumor-to-blood (T/B) (5.48 ± 0.12) ratios at 1 h post injection in A375-hPD-L1 tumor-bearing mice (Supplemental Fig. 10). Although the T/M ratio decreased slightly to 6.76 ± 0.41 at 2 h post injection, the T/B ratio increased to 7.07 ± 0.11. In contrast, at 2 h post injection both the T/M (0.98 ± 0.21) and T/B (2.87 ± 0.13) ratios in MCF-7 tumor-bearing mice were still very low. In addition, more than 90% intact ^{68}Ga-NOTA-Nb109 in the urine was detected at 2 h post injection, further demonstrating the high in vivo stability of the nanobody (Supplemental Fig. 2).

DISCUSSION

As immunotherapy targeted PD-1/PD-L1 pathway shows impressive clinical outcomes, several radiolabeled imaging agents of PD-L1 have been reported recently (*13-20*). They allow for a visualization of PD-L1 status in patients before, during and after therapeutic intervention, and could guide the clinical treatment. Recently nanobodies have shown very promising results as imaging agents for their favorable physicochemical properties, such as small size, high stability, rapid tumor uptake and

normal tissue clearance. In order to facilitate the protein isolation, nanobodies are often modified with a His-tag during the protein production, which in turn lead to the high kidney uptake and increasing risk for immunogenicity. These have become obstacles to their clinical applications (*28*). Therefore, a ^{68}Ga-labeled nanobody based probe ^{68}Ga-NOTA-Nb109 without the His-tag was designed and prepared in high purity and stability, which held great potential for PET imaging of PD-L1 expression in cancers.

The binding assay proved the strong binding ability of Nb109 to PD-L1, which possessed a K_D value comparable with most reported PD-L1 antibodies (*12*). Furthermore, the similar binding curves of ^{69}Ga-NOTA-Nb109 and Nb109 to PD-L1 demonstrated the strong binding ability of ^{69}Ga-NOTA-Nb109 to PD-L1, and also indicated that the conjugation of chelator NOTA with $^{68}Ga^{3+}$ had no effect on the affinity of Nb109 for PD-L1. Six-fold higher uptake of radioactivity in A375-hPD-L1 cells than that in MCF-7 cells further confirmed the specificity of ^{68}Ga-NOTA-Nb109 for PD-L1. All the results demonstrate that the tracer ^{68}Ga-NOTA-Nb109 binds tumor cells in vitro in a PD-L1 expression-dependent manner.

Compared with most nanobody-based imaging agents with the histidine tag reported previously (*29*), our tracer ^{68}Ga-NOTA-Nb109 showed much lower kidney retention due to the lack of histidine tag, which can be seen from the PET imaging and biodistribution studies. A higher tumor uptake in A375-hPD-L1 bearing mice than that in MCF-7 bearing mice was observed, which was contributed to the overexpression of PD-L1 in A375-hPD-L1 tumor. This demonstrated that the tracer ^{68}Ga-NOTA-Nb109 could

specifically bind with PD-L1 in vivo. The retention of radioactivity in tumor remained relatively stable for 2 h, but fast cleared from the muscle and blood, which resulted in a high tumor-to-background ratio in A375-hPD-L1 tumor. Owing to the low uptake in MCF-7 tumor, the tumor-to-background ratio was correspondingly low and tumors were not visible throughout the imaging process.

Competitive binding assay indicated that the in vitro binding of Nb109 to PD-L1 was not influenced by PD-1 or KN035 even under 1000-fold excess, but it could be blocked nearly 80% by the same amount of unlabeled Nb109. This demonstrated the different binding epitopes between Nb109 and PD-1 or PD-L1 antibody as well as the specificity of the tracer. For in vivo study, it also confirmed that there was also no impact on the tumor uptake of ^{68}Ga-NOTA-Nb109 before and after injection of KN035, since comparable tumor uptake and images were obtained. This demonstrated the different binding sites of ^{68}Ga-NOTA-Nb109 and anti-PD-L1 antibodies to PD-L1. The non-blocking binding property of ^{68}Ga-NOTA-Nb109 endowed it great potential for detection of PD-L1 and evaluation of the prognosis in clinical, as it could avoid the effect of anti-PD-L1 antibodies in the course of treatment.

Comparison of PET images of three types of tumor-bearing mice clearly revealed that the tracer ^{68}Ga-NOTA-Nb109 tended to accumulate in A375-hPD-L1 tumors owing to the high PD-L1 expression. For A375-hPD-L1/A375 tumor, the PD-L1 expression decreased because of the doping of A375 cells, and thus the uptake of ^{68}Ga-NOTA-Nb109 decreased as anticipated. Moreover, since A375 cells had a low

PD-L1 expression, A375 tumor was not visible throughout the scanning. This was further confirmed by immunohistochemistry and autoradiography of tumors post imaging. All the results indicated that ^{68}Ga-NOTA-Nb109 could selectively accumulate in PD-L1-positive A375-hPD-L1 tumor and rapidly clear from the muscle and blood, resulting in a high tumor-to-background ratio.

CONCLUSIONS

A novel ^{68}Ga-labeled nanobody ^{68}Ga-NOTA-Nb109 was developed for PET imaging of PD-L1 in vivo. It was generated with high affinity toward PD-L1 in high radiochemical yield and radiochemical purity. The tracer showed selective accumulation in PD-L1-positive tumors and rapid clearance from the muscle and blood, resulting in a high tumor-to-background ratio. All the results indicated that ^{68}Ga-NOTA-Nb109 had great potential for PD-L1 detection, evaluating the curative effect, and optimizing the prescription for PD-1/PD-L1 checkpoint blockade therapy.

DISCLOSURE

The authors declare no conflict of interest.

ACKNOWLEDGEMENTS

This work was financially supported by National Natural Science Foundation of China (21501074), Natural Science Foundation of Jiangsu Province (BK20181128), the 333 Project of Jiangsu Province (BRA2016518, LGY2018086), the Key Youth Medical Talent Project of Jiangsu Province (QNRC2016626 and QNRC2016629), the Science Technology Development Project of Wuxi

(WX18IIAN049) and the Precision Medical Project of Wuxi Commission of Health and Family Planning (J201806).

KEY POINTS

QUESTION: How to detect programmed death ligand 1 (PD-L1) expression rapidly and accurately in living subjects?

PERTINENT FINDINGS: A novel nanobody based PET tracer ^{68}Ga-NOTA-Nb109 was developed with high affinity for PD-L1. PET imaging studies on the tumor-bearing models with high, medium and low PD-L1 expression demonstrated that the tracer could distinctly distinguish different tumors and noninvasively quantify the PD-L1 expression in tumors.

IMPLICATIONS FOR PATIENT CARE: The tracer ^{68}Ga-NOTA-Nb109 holds great potential for PD-L1 detection, evaluating the immunotherapeutic effect and optimizing the prescription for PD-1/PD-L1 checkpoint blockade therapy.

REFERENCES

1. Francis DM, Thomas SN. Progress and opportunities for enhancing the delivery and efficacy of checkpoint inhibitors for cancer immunotherapy. *Adv Drug Deliv Rev*. 2017;114:33-42.

2. Ohaegbulam KC, Assal A, Lazar-Molnar E, et al. Human cancer immunotherapy with antibodies to the PD-1 and PD-L1 pathway. *Trends Mol Med*. 2015;21:24-33.

3. Bellmunt J, Powles T, Vogelzang NJ. A review on the evolution of PD-1/PD-L1 immunotherapy for bladder cancer: The future is now. *Cancer Treat Rev*. 2017;54:58-67.

4. Zhang F, Wei H, Wang X, et al. Structural basis of a novel PD-L1 nanobody for immune checkpoint blockade. *Cell Discov.* 2017;3:17004-17016.

5. Emens LA, Ascierto PA, Darcy PK, et al. Cancer immunotherapy: Opportunities and challenges in the rapidly evolving clinical landscape. *Eur J Cancer.* 2017;81:116-129.

6. Zhan M, Hu X, Liu X, et al. From monoclonal antibodies to small molecules: the development of inhibitors targeting the PD-1/PD-L1 pathway. *Drug Discov Today*. 2016;21:1027-1036.

7. Geng Q, Jiao P, Jin P, et al. PD-1/PD-L1 Inhibitors for immuno-oncology: From antibodies to small molecules. *Curr Pharm Des.* 2017;23:1-9.

8. Hettich M, Braun F, Bartholomä MD, et al. High-resolution PET imaging with therapeutic antibody-based PD-1/PD-L1 checkpoint tracers. *Theranostics.* 2016;6:1629-1640.

9. England CG, Ehlerding EB, Hernandez R, et al. Preclinical pharmacokinetics and

biodistribution studies of ^{89}Zr-Labeled pembrolizumab. *J Nucl Med.* 2017;58:162-168.

10. Du Y, Liang X, Li Y, et al. Nuclear and fluorescent labeled PD-1-liposome-DOX-^{64}Cu/IRDye800CW allows improved breast tumor targeted imaging and therapy. *Mol Pharm.* 2017;14:3978-3986.

11. Natarajan A, Mayer AT, Xu L, et al. Novel Radiotracer for immunoPET imaging of PD-1 checkpoint expression on tumor infiltrating lymphocytes. *Bioconjugate Chem*. 2015;26:2062-2069.

12. González Trotter DE, Meng X, McQuade P, et al. In vivo imaging of the programmed death ligand 1 by ^{18}F positron emission tomography. *J Nucl Med*. 2017;58:1852-1857.

13. Donnelly DJ, Smith RA, Morin P, et al. Synthesis and biological evaluation of a novel ^{18}F-labeled adnectin as a PET radioligand for imaging PD-L1 expression. *J Nucl Med*. 2017;59:529-535.

14. Mayer AT, Natarajan A, Gordon SR, et al. Practical immuno-PET radiotracer design considerations for human immune checkpoint imaging. *J Nucl Med*. 2017;58:538-546.

15. Truillet C, Oh HLJ, Yeo SP, et al. Imaging PD-L1 expression with immunoPET. *Bioconjugate Chem*. 2018;29:96-103.

16. Chatterjee S, Lesniak WG, Miller MS, et al. Rapid PD-L1 detection in tumors with PET using a highly specific peptide. *Biochem Biophys Res Comm*. 2017;483:258-263.

17. De Sliva RA, Kumar D, Lisok A, et al. Peptide-based ^{68}Ga-PET radiotracer for imaging PD-L1 expression in cancer. *Mol Pharm.* 2018;15:3946-3952.

18. Kumar D, Lisok A, Dahmane E, et al. Peptide-based PET quantifies target engagement of PD-L1 therapeutics. *J Clin Ivenst.* 2019;129:616-630.

19. Lesniak WG, Chatterjee S, Gabrielson M, et al. PD-L1 detection in tumors using [^{64}Cu]atezolizumab with PET. *Bioconjugate Chem*. 2016;27:2103-2110.

20. Natarajan A, Patel CB, Habte F, et al. Dosimetry prediction for clinical translation of ^{64}Cu-pembrolizumab immunoPET targeting human PD-1 expression. *Sci Rep.* 2018;8:633-644.

21. England CG, Jiang D, Ehlerding EB, et al. ^{89}Zr-labeled nivolumab for imaging of T-cell infiltration in a humanized murine model of lung cancer. *Eur J Nucl Med Mol I.* 2018;45:110-120.

22. Schumacher D, Helma J, Schneider AFL, et al. Nanobodies: chemical functionalization strategies and intracellular applications. *Angew Chem Int Ed.* 2018;57:2134-2333.

23. Wang Q, Lou W, Di W, et al. Prognostic value of tumor PD-L1 expression combined with CD8+ tumor infiltrating lymphocytes in high grade serous ovarian cancer. *Int Immuno Pharmacol.* 2017;52:7-14.

24. Bailly C, Cléry P, Faivre-Chauvet A, et al. Immuno-PET for clinical theranostic approaches. *Inter J Mol Sci*. 2017;18:57-69.

25. Lindmo T, Boven E, Cuttitta F, et al. Determination of the immunoreactive fraction of radiolabeled monoclonal antibodies by linear extrapolation to binding at infinite antigen excess. *J Immunol Methods*. 1984;72:77-89.

26. Li D, Cheng S, Zou S, et al. Immuno-PET imaging of ^{89}Zr labeled anti-PD-L1 domain antibody. *Mol Pharm.* 2018;15:1674-1681.

27. Zhou Z, Vaidyanathan G, McDougald D, et al. Fluorine-18 labeling of the HER2-targeting single-domain antibody 2Rs15d using a residualizing label and preclinical evaluation. *Mol Imaging Biol.* 2017;19:867-877.

28. Xavier C, Vaneycken I, D'huyvetter M, et al. Synthesis, preclinical validation, dosimetry, and toxicity of ^{68}Ga-NOTA-Anti-HER2 nanobodies for iPET maging of HER2 receptor expression in cancer. *J Nucl Med*. 2013;54:776-784.

29. Broos K, Keyaerts M, Lecocq Q, et al. Non-invasive assessment of murine PD-L1 levels in syngeneic tumor models by nuclear imaging with nanobody tracers. *Oncotarget*. 2017;8:41932-41946.

FIGURES

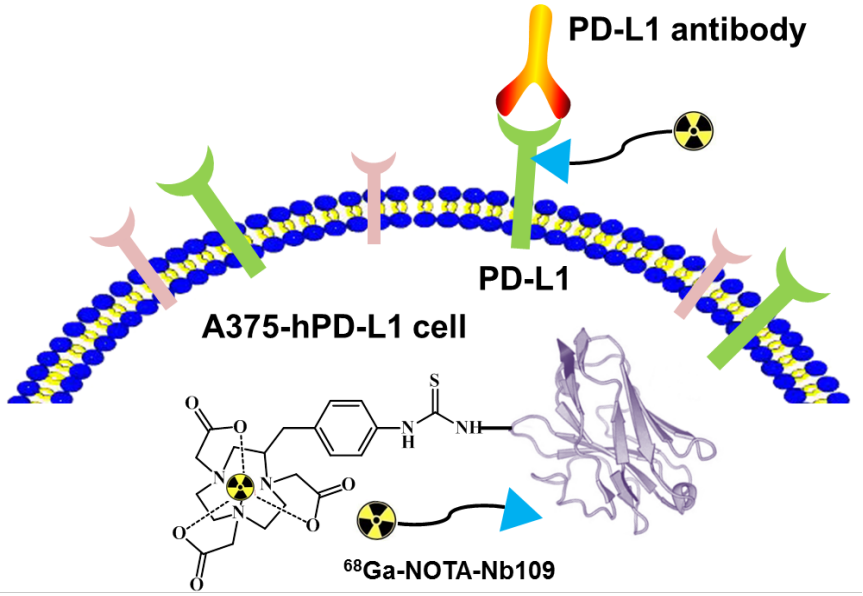

FIGURE 1 Schematic illustration of ^{68}Ga-NOTA-Nb109 binding with PD-L1.

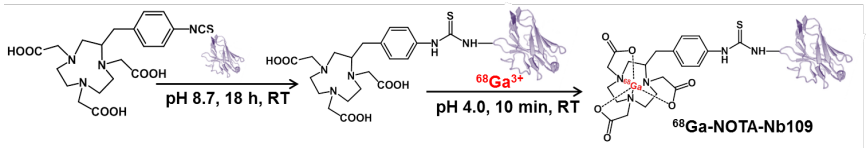

FIGURE 2 Synthetic scheme of ^{68}Ga-NOTA-Nb109.

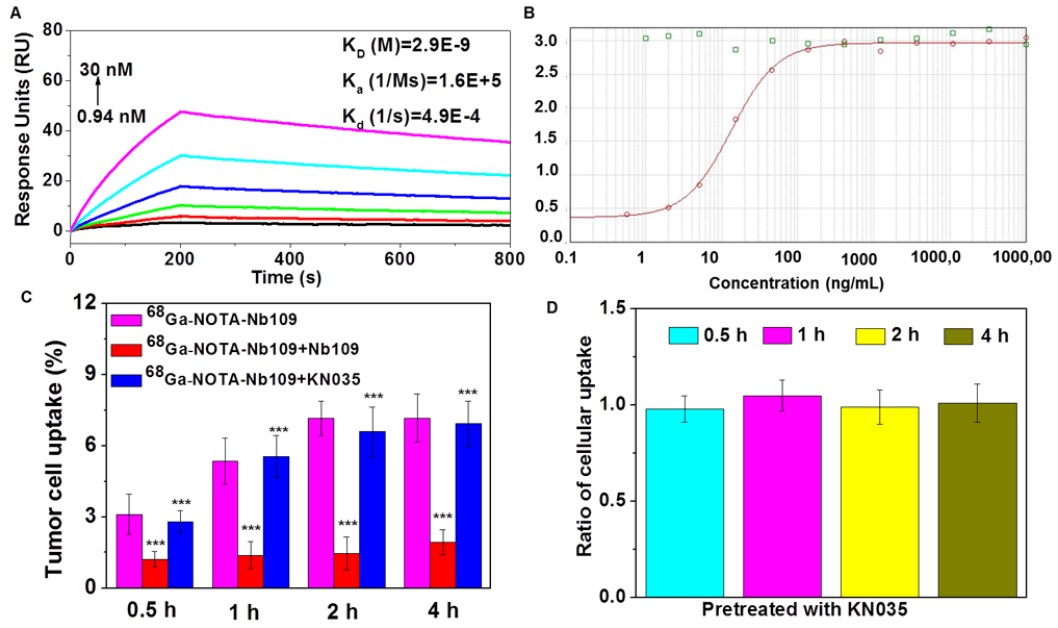

FIGURE 3 In vitro binding studies. (A) Affinity/kinetics surface plasmon resonance study of Nb109 interacting with immobilized recombinant human PD-L1 protein. (B) Binding curves of Nb109 (red) to PD-L1 at the presence of PD-1 (green). (C) The uptake of ^{68}Ga-NOTA-Nb109 in A375-hPD-L1 with or without pretreatment of 1000-fold unlabeled Nb109 or KN035 at different time. (D) The ratio of cellular uptake of ^{68}Ga-NOTA-Nb109 in A375-hPD-L1 before and after pretreatment with 1000-fold KN035 for 0.5, 1, 2 and 4 h. *** $P < 0.001$ vs ^{68}Ga-NOTA-Nb109

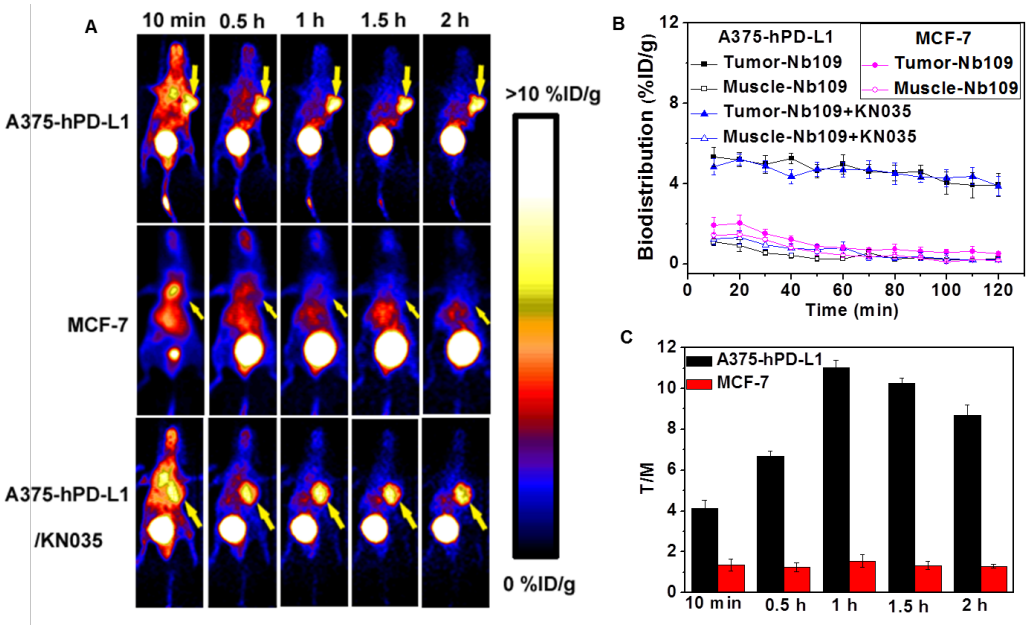

FIGURE 4 MicroPET imaging studies of tumor-bearing models (n = 3). (A) Dynamic PET scanning of A375-hPD-L1 (with or without injection of KN035) and MCF-7 tumor-bearing models over 0-2 h post injection of 4.0-5.0 MBq of ^{68}Ga-NOTA-Nb109. (B) and (C) Biodistribution of ^{68}Ga-NOTA-Nb109 and tumor-to-muscle (T/M) ratio analyzed according to the quantification analysis of PET images.

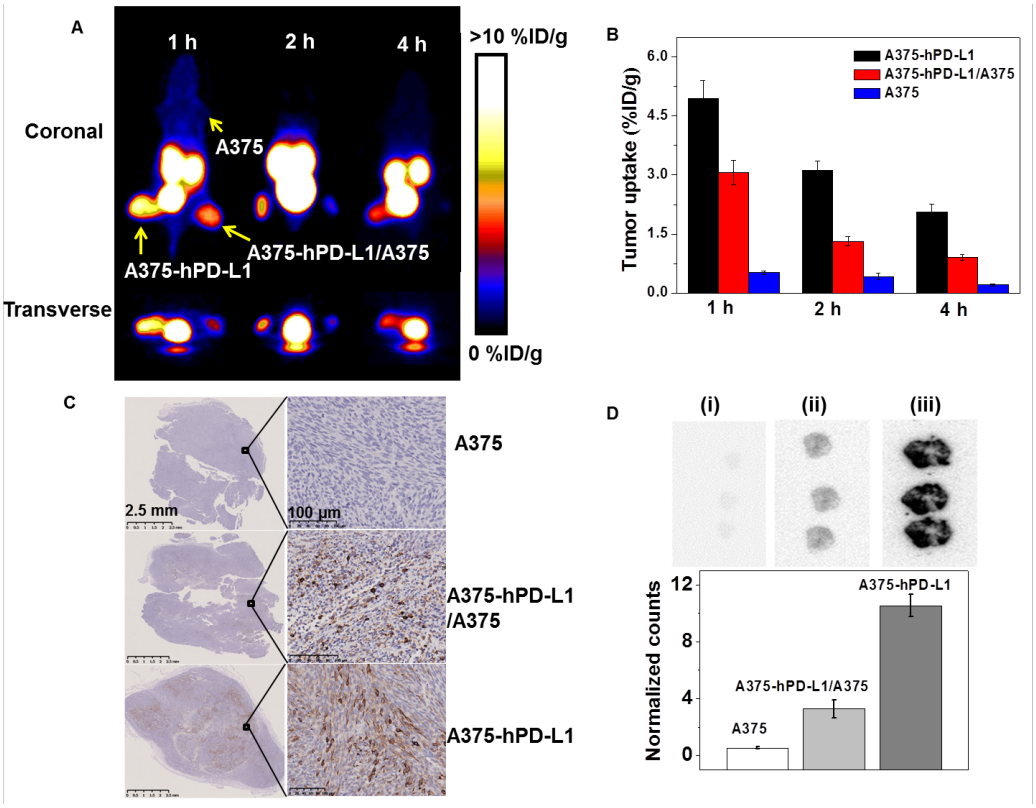

FIGURE 5 MicroPET imaging of the tumor-bearing models. (A) Static microPET images at 1, 2 and 4 h post injection of 2.5 MBq of ^{68}Ga-NOTA-Nb109 (n = 3). (B) Uptake of ^{68}Ga-NOTA-Nb109 in tumors according to the quantification analysis of PET images. (C) The PD-L1 immunohistochemical staining of the tumors (n = 5, scale bar = 2.5 mm in left column and 100 μm in right column). (D) The autoradiography analysis of ^{68}Ga-NOTA-Nb109 in A375 (i), A375/A375-hPD-L1 (ii) and A375-hPD-L1 (iii) tumor (up) and quantitative analysis of autoradiography (bottom).

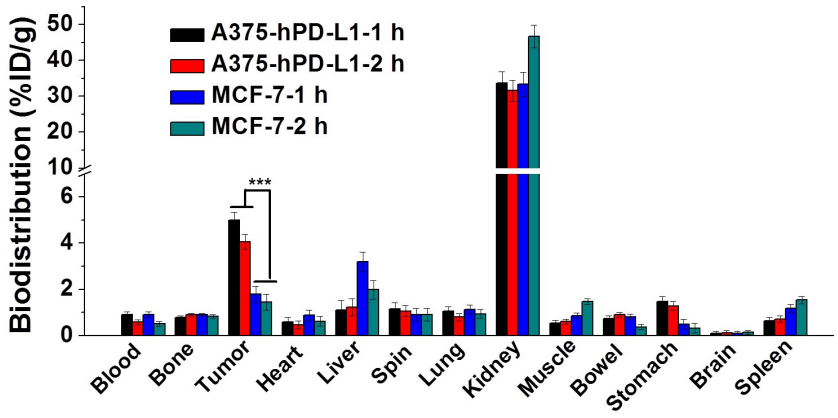

FIGURE 6 Biodistribution analysis at 1 h and 2 h post injection of ^{68}Ga-NOTA-Nb109 in A375-hPD-L1 and MCF-7 tumor-bearing models (n = 5). ***, $p < 0.001$.

Supplemental Figure 1

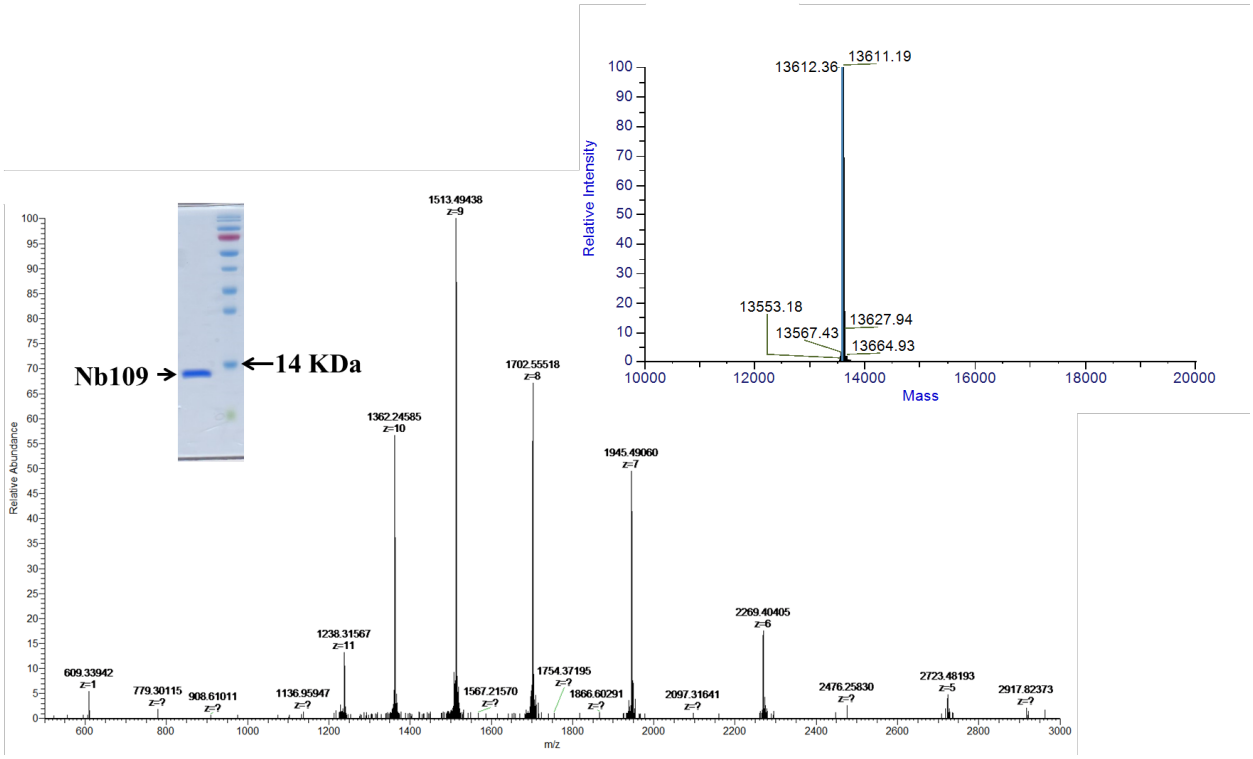

Supplemental Figure 1 The SDS-PAGE and ESI-Q-TOF-MS characterization of Nb109.

Supplemental Figure 2

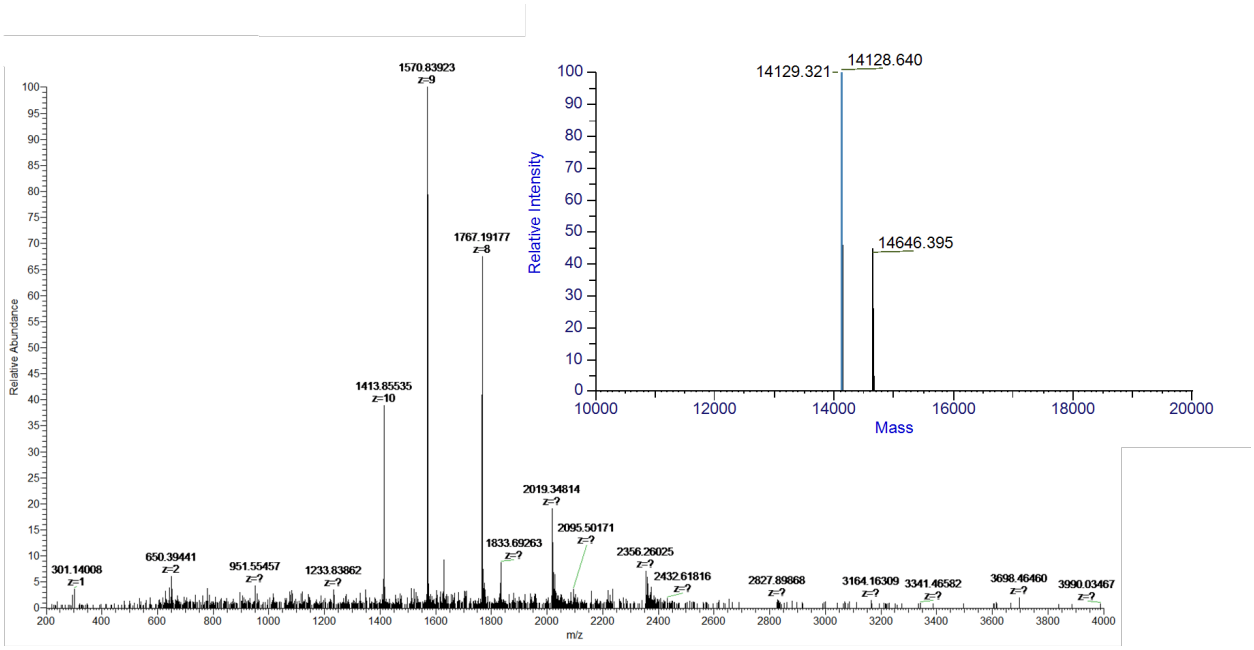

Supplemental Figure 2 The ESI-Q-TOF-MS of NOTA-Nb109.

Supplemental Figure 3

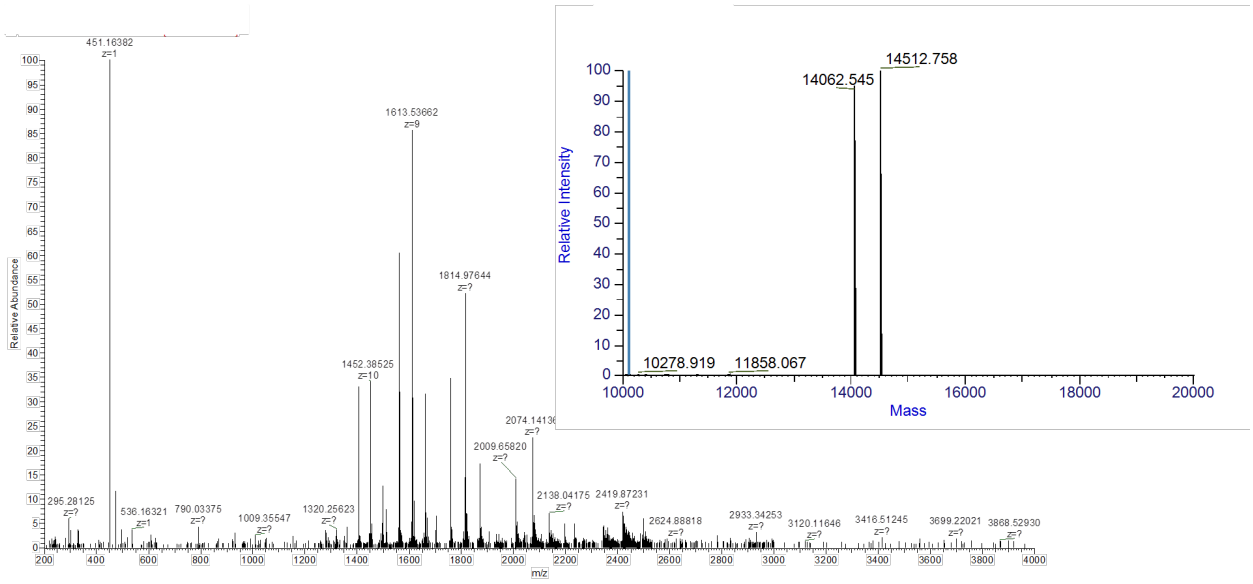

Supplemental Figure 3 The ESI-Q-TOF-MS of ^{69}Ga-NOTA-Nb109.

Supplemental Figure 4

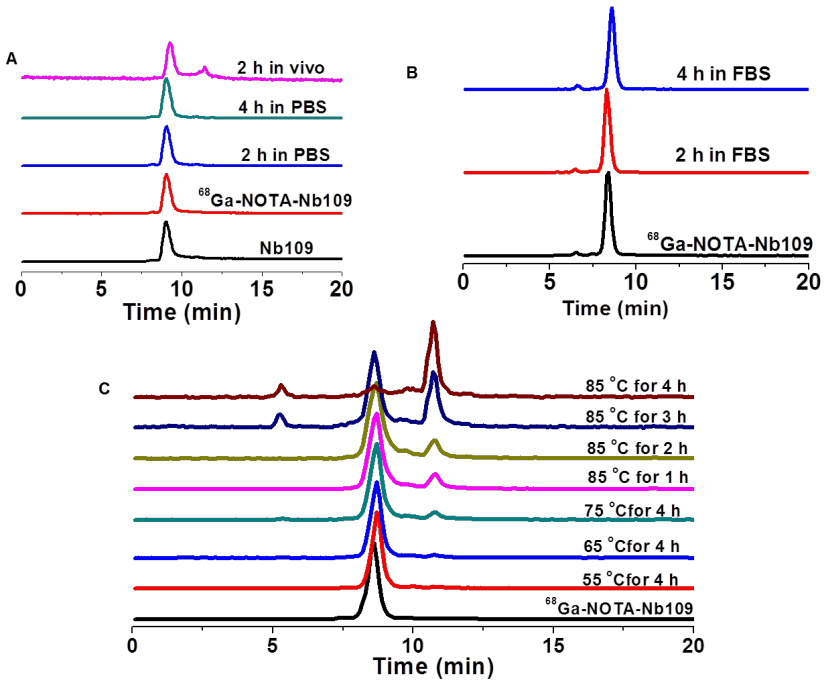

Supplemental Figure 4 In vitro stability of ^{68}Ga-NOTA-Nb109 in (A) PBS (pH 7.4) and urine and (B) fetal bovine serum (FBS) at different time under 37 °C; (C) the thermal stability of ^{68}Ga-NOTA-Nb109 under different temperature. Nb109: UV detector (320 nm), ^{68}Ga-NOTA-Nb109: radioactive detector.

Supplemental Figure 5

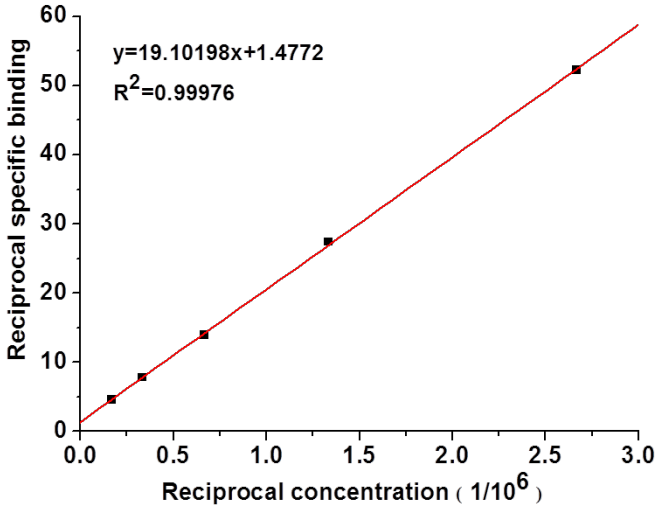

Supplemental Figure 5 The immunoreactivity assay of ^{68}Ga-NOTA-Nb109.

Supplemental Figure 6

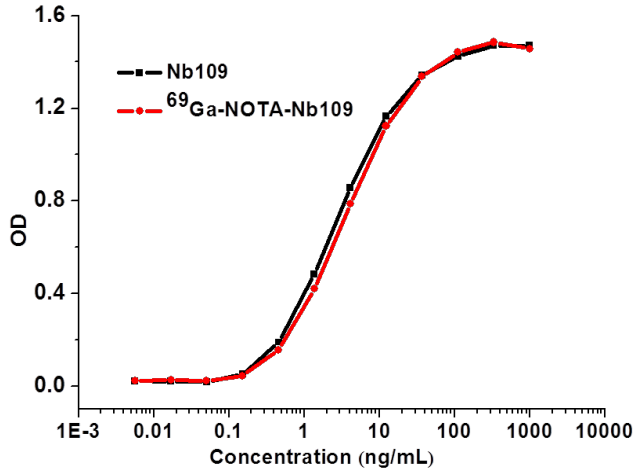

Supplemental Figure 6 The binding curves of Nb109 (black) and ^{68}Ga-NOTA-Nb109 (red) to PD-L1 assessed by ELISA.

Supplemental Figure 7

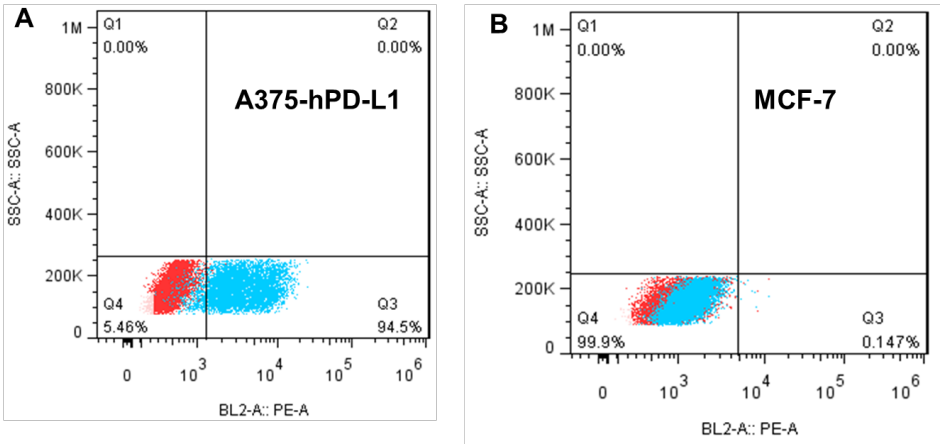

Supplemental Figure 7 The expression of PD-L1 in A375-hPD-L1 (A) and MCF-7 (B) cell lines measured by flow cytometry.

Supplemental Figure 8

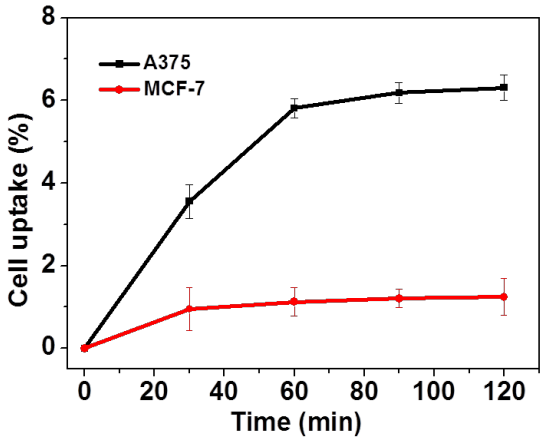

Supplemental Figure 8 The cellular uptake of ^{68}Ga-NOTA-Nb109 in A375-hPD-L1 (black) and MCF-7 (red) cell lines at different time points.

Supplemental Figure 9

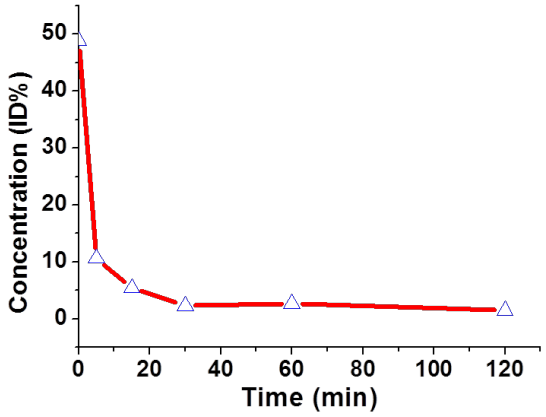

Parameter	Unit	Value
$t_{1/2}$	min	49.79
T_{max}	min	0.10
C_{max}	ID%	48.82
C_0	ID%	50.37
AUC_{0-t}	ID%*min	487.03
AUC_{0-inf}	ID%*min	593.39
MRT_{0-inf}	min	60.53
V_z	(μci)/(ID%)	11.41
CL	(μci)/(ID%)/min	0.15
V_{ss}	(μci)/(ID%)	9.61

Supplemental Figure 9 The pharmacokinetic behavior of ^{68}Ga-NOTA-Nb109.

Supplemental Figure 10

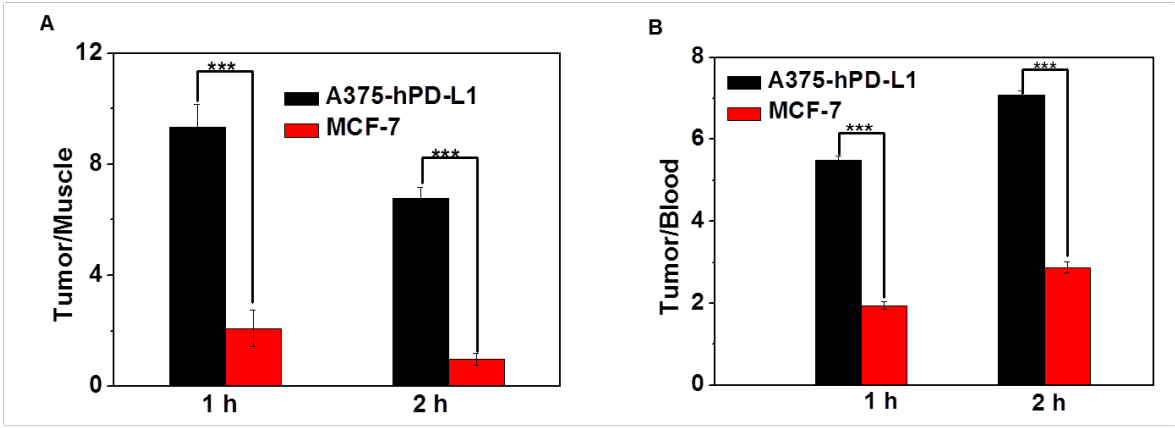

Supplemental Figure 10 The tumor-to-muscle (A) and tumor-to-blood (B) ratios at 1 h and 2 h post injection of ^{68}Ga-NOTA-Nb109 in tumor-bearing models, respectively. ***, $p < 0.001$..